ROSAT PSPC observations of 5 X-ray bright early type galaxies

G. Trinchieri[1,2]**, G. Fabbiano**[3]**, and D-W. Kim**[4]

[1] Osservatorio Astronomico di Brera, Via Brera 28, I-20121 Milano, Italy
[2] Visiting Astronomer, Max-Planck Institut für extraterrestrische Physik, Garching bei München, Germany
[3] Harvard-Smithsonian Center for Astrophysics 60 Garden St., Cambridge, MA 02138, USA
[4] Chungnam National University, Dept. of Astron. and Space Sci., 305-764 Daejeon, Korea

Abstract. We report on the ROSAT PSPC observations of 5 X-ray bright early-type galaxies. Their X-ray morphology is more complex than $Einstein$ data had shown, ranging from the ellipsoidal shape of NGC 533 to the ~ 200 kpc tail of NGC 7619. Hot gas at an average temperature of 0.8-1 keV dominates their X-ray emission. The spectral analysis is based on the assumption of a hot thin plasma at cosmic abundances, since the spectral resolution of the PSPC does not allow unambiguous measures of the model parameters (temperatures, low energy cut-off, metal abundance). However, the estimated temperature are not strongly affected by this choice. A temperature distribution of the hot interstellar medium is also derived. Higher temperatures are in some cases observed at larger radii, while the innermost $1'$ region is cooler in all of the objects studied. Due to the large range in distances however this corresponds to significantly different galaxy radii, from 5 kpc in NGC 4649 to 30 kpc in NGC 533.

The temperature and density distributions derived are used to estimate the total mass of these systems, which span from $M_T \sim 10^{12} - 10^{13}$ $M_\odot$ and corresponding mass-to-light ratios M/L $\sim$ 10-150 in solar units. Formal errors on the derived masses are estimated to be $> 25\%$.

Care must be taken in comparing results for different systems, since some of the emission attributed to these objects could suffer from the contribution for the groups and clusters they belong to. Accordingly, our mass estimates could reflect the effect of the cluster/group potential.

Send offprint requests to: G. Trinchieri

1. Introduction

$Einstein$ observations of early type galaxies have established that a hot interstellar medium (ISM) dominates the emission in the X-ray brightest objects. This discovery is very important for many reasons: 1) it has indicated the presence of substantial amounts of ISM in these objects; 2) it has provided a potentially powerful tool for estimating total galaxy masses at large radii; 3) it has provided a new wealth of parameters for the understanding of the enrichment of the intercluster medium. However, with $Einstein$ data, we had not been able to achieve a good understanding of the detailed properties of the hot ISM. Average spectral parameters, over the entire source extent, could be estimated, albeit with large uncertainties. The morphological appearance and total extent of the hot ISM could only be roughly estimated.

The improved spatial and spectral resolution of the PSPC (Position Sensitive Proportional Counter) instrument on board the ROSAT satellite (Trümper 1983; Pfeffermann et al 1987) has proven to be crucial in furthering our understanding of the properties of the X-ray emitting gas in early type, normal, nearby galaxies. Its softer energy band ($\sim 0.1 - 2$ keV) coupled with the $\leq 0.5'$ spatial resolution is well suited for studying the spectral parameters of the gas in $\sim 1'$ annular regions. This approach has already been successfully applied to the data of other X-ray bright early type galaxies ($e.g.$ NGC 4636, Trinchieri et al 1994; NGC 507, Kim & Fabbiano 1995 among others). This work suggests that that the hot ISM is not isothermal over the entire source, but can show a slow temperature increase over a large region (~ 40 kpc in NGC 4636), and that its morphology is far from smooth and regular, but can show asymmetries and inhomogeneities ($e.g.$ NGC 507).

In order to better understand the characteristics of the ISM in early type galaxies we have observed 5 X-ray bright early type galaxies for which $Einsetin$ data had already established the presence of a dominating hot gas component in their X-ray emission. The environment in which the galaxies sit spans a large range in richness, from the low density environment of NGC 533 (in the vicinity of A193, it is at the same recessional

Table 1. Log of the Observations

Field	RA Dec (J2000)	Obs. Dates Beginning End	On Time (s)
NGC 533	1:25:31.2 1:45:36.0	14/07/93 27/07/93	13054
NGC 2563	8:20:36.0 21:04:12.0	11/10/93 13/10/93	27174
		30/04/94 02/05/94	22873
NGC 4649	12:43:43.2 11:33:36.0	21/12/91 27/12/91	14301
NGC 7619/7626 (Pegasus I)	23:20:31.2 8:12:36.0	30/05/92 11/06/92	18234

Table 2. Parametric Representation of Radial Distribution of the X-ray Surface Brightness outside $r \sim 2'$

Galaxy	R_{max}^a	α
NGC 533	16′	-1.95 ± 0.14^b
NGC 2563	14′	-1.18 ± 0.07
NGC 4649	13′	-2.51 ± 0.18
	7′	-3.39 ± 0.25
NGC 7619	22′	-1.45 ± 0.06^b
		-1.28 ± 0.17^c
NGC 7626	3.′5	-2.87 ± 0.05^d

[a] Maximum radius used in the fit
[b] For the azimuthally averaged profile
[c] From 4′ to 22′, in the 250^o pie region that excludes the X-ray tail
[d] From 1.5′ to 3.′5 only.

velocity but it is located at $> 3°$, or > 6 Mpc, from the cluster center, and it is not considered as a possible member, Chapman et al 1988; it is instead one of 4 members of group GH14, Geller & Huchra 1983) to galaxies in groups and poor clusters (NGC 7619 and NGC 7626 in Pegasus I group; NGC 2563 in group A of the Cancer cluster) and galaxies in richer clusters (NGC 4649 in the Virgo cluster, at ≥ 1 Mpc from the cluster center).

The five early type galaxies have been observed by the ROSAT PSPC as summarized in Table 1. The two observations of NGC2563 have been merged to improve on the statistical significance of the data, after checking that the single observations yielded consistent results. The data have been analyzed using primarily the PROS software available under IRAF. The details of the spatial and spectral analysis are reported in Sect. 2. Derived quantities are discussed in Sect. 3. Sects. 4–6 are devoted to the results for the Pegasus I and Cancer groups. The general results of these observations are summarized in the conclusions.

2. Data analysis

The early type galaxies considered here all show extended emission in X-rays. Contour plots of their smoothed images in the energy band 0.14-2.0 keV are shown in Fig. 1, 8 and 9. In this energy band the expected effect of the vignetting correction is well represented by the exposure map (a model field containing information about the effective exposure moduled by the expected vignetting, see PSPC documentation for more details) provided with the data for each observed field (see also Trinchieri et al 1994, Kim & Fabbiano 1995). We can therefore use this map to flat field the data.

The raw images have been normalized to the exposure maps, and smoothed with a Gaussian function, as specified in the figure caption. Several additional sources are visible, often embedded in the X-ray emission of the target galaxy. These possible interlopers were conservatively excluded from the subsequent analysis, unless otherwise noted, by masking out circles at the source positions with radii chosen to be comparable to the outer contour (typically at 2σ) on the contour maps. The presence of

several, possibly unrelated, sources in the field is not surprising. From the LogN-LogS function derived from ROSAT data (Hasinger et al 1993) we can estimate that ~ 6 sources will be present in the inner ~ 0.3 square degree field at $f_x \geq 4 \times 10^{-14}$ erg cm^{-2} s^{-1}, and ~ 20 if the flux limit is lowered to 2×10^{-14} erg cm^{-2} s^{-1}.

The NGC2563, NGC4649 and NGC7626 images show extended and azimuthally symmetric emission. The external X-ray isophotes of the NGC533 map instead show a more elliptical shape. A tail of emission is observed to the SW of NGC7619, extending for about 10′ away from the X-ray peak.

2.1. Radial count distribution

To estimate the size of the X-ray sources associated with these galaxies, we have produced plots of the radial distribution of the X-ray emission and compared them with the expected background, estimated from the properly normalized corresponding exposure map (Fig. 2). We have used concentric annuli, centered at the source peak position, with width varying from 0.25′ to $2' - 3'$ depending on the counting statistics. The profile of the Pegasus I group is centered on NGC 7619.

It appears that the profile of the NGC4649 field has the same shape as the exposure map from $r \sim 10'$. However, two different normalizations are necessary to match the level of emission, one in the $\sim 10' - 16'$ annulus and a lower one outside of $\sim 25'$ (both shown in the figure). A more careful determination of the shape and level of the background will be necessary for this object; however, in this work we will consider both possibilities and will discuss the differences in the two cases.

As can be seen from Fig. 2, the exposure map represents a good fit to the emission in the region outside $\sim 20'$ from the field center (e.g. outside of the ring of the support structure for the PSPC that has a shape reminiscent of a "wagon wheel" and that can be recognized as a "dip" in both source data and exposure map profiles).

The net count distributions are plotted in Fig. 3 to 5 for each galaxy. Two Point Spread Functions (PSF), one appropriate for on-axis sources with temperatures of 0.2 keV (the softest
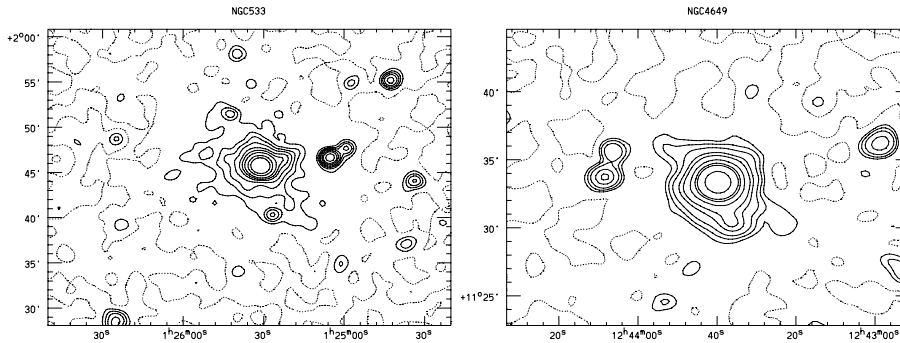
Fig. 1. Isointensity contour plots of NGC 533 and NGC 4649. Data in the 0.14-2.0 keV energy range have been normalized by the exposure map, and smoothed with a Gaussian function with $\sigma = 30''$. A constant background value has been subtracted. The dashed contour is for 0 counts. Other contours are at 2σ, 3σ, 4σ, 5σ, and higher.
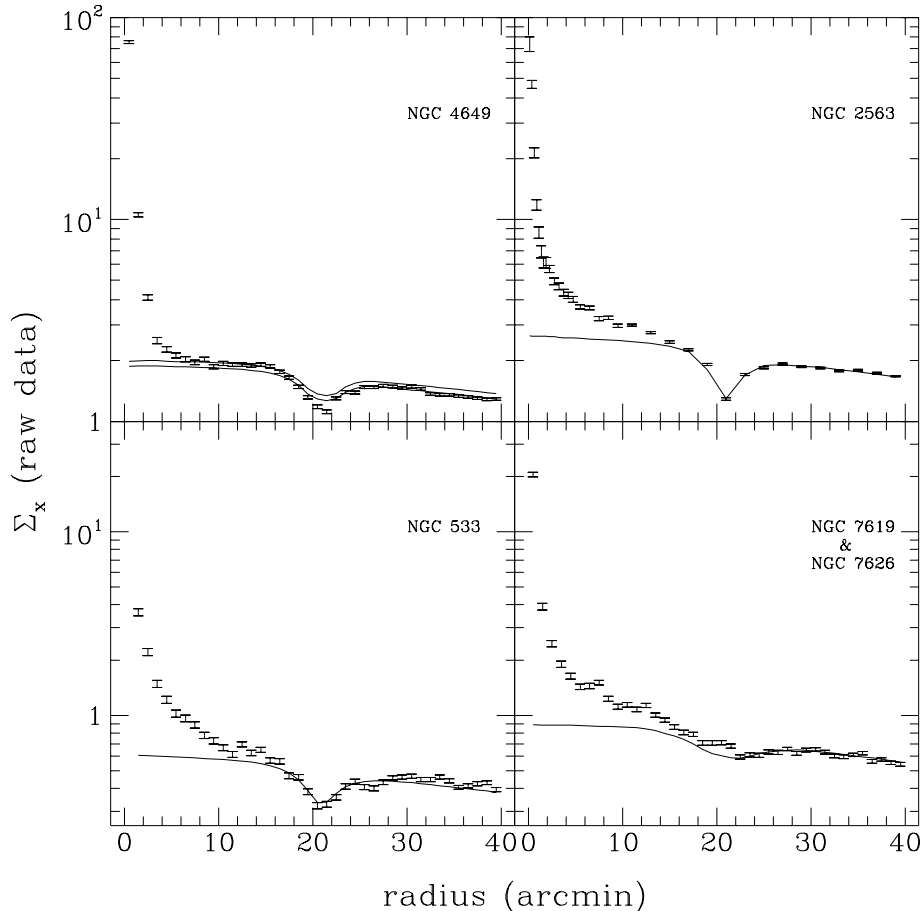
Fig. 2. Radial surface brightness distribution of the raw counts, in concentric annuli centered at the X-ray peak position (coincident with the optical position of the galaxy's nucleus). The solid line represents the background model we have assumed for each field, derived from the exposure map properly rescaled to the data. The two lines shown for NGC 4649 represent two different normalization values (see text). The profile of NGC 7619 & NGC 7626 is centered on NGC7619, offset from the field's center. Consequently, the "dip" in the exposure map profile here is not as pronounced as in the other cases.

PSF available with the PROS software) and one for a kT corresponding to the best fit temperature of the innermost circle (see Sect. 2.2), are also plotted for comparison, normalized at the central bin. In all cases the emission is clearly larger than either PSF, although in most cases the 0.2 keV PSF is a reasonable representation of the data for r$\leq$ 1'. The spectral results however indicate significantly harder emission in that region (cf. Sect. 2.2).

Fig. 4 and 5 show both the azimuthally averaged profiles of NGC533 and NGC7619 and the comparison of the emissions from different pie regions. In NGC 533 there is an indication of a significant change of slope at r$\sim$ 1'. This could be interpreted as due to the presence of an unresolved, very soft core, since the emission within 1' radius is well approximated by the 0.2

keV PSF. However, this is in contrast with the spectral results (Sect. 2.2), that indicate an average kT of 0.9 keV in the inner 1' circle. More likely, the difference is due to the dominating contribution of the galaxy relative to the group emission (1' $\sim$ 30 kpc at the galaxy's distance).

Fig. 4b compares the NE-SW sectors averaged together (i.e. a 70° cone along position angle PA=35°, counterclockwise from North) to that in the NW-SE ones (PA=125°). Outside of r$\sim$ 5' − 6', the surface brightness along PA=35° is flatter and significantly higher than that from the complementary regions.

In Fig. 5b, the region SW of NGC7619 (from 170° to 280°, corresponding to the 'tail' visible in the contour plot of Fig. 8), and the complementary region are compared. The SW profile appears significantly higher than in the other angular sector for
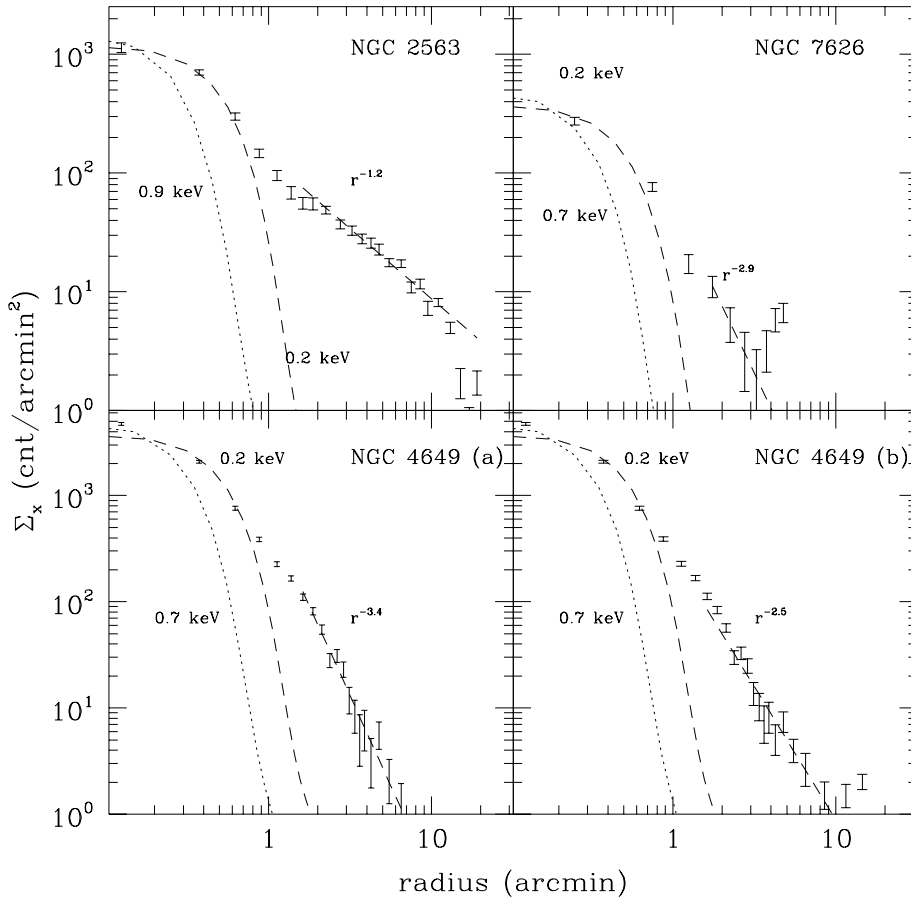
Fig. 3. Radial surface brightness profile of the net X-ray emission, in concentric circular annuli, for NGC 2563, NGC 4649 and NGC 7626. The power law fits of Table 2 are reported on the data.
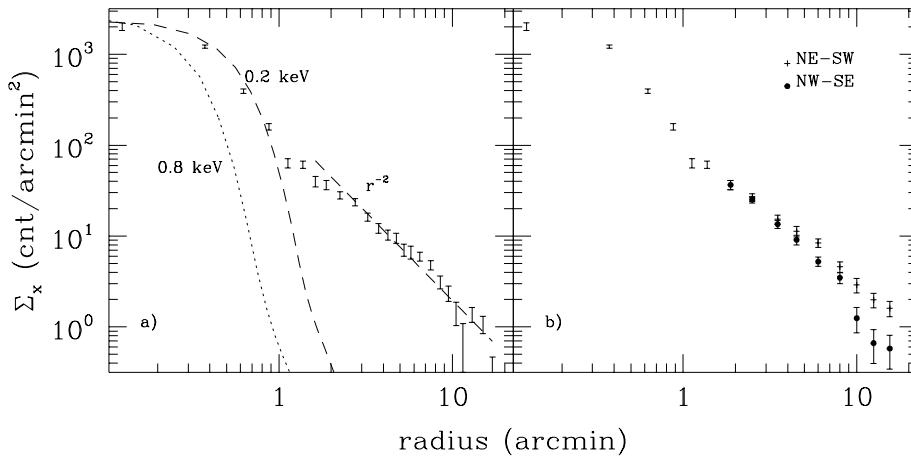
Fig. 4a and b. Radial surface brightness profile of the net X-ray emission of NGC533, azimuthally averaged **a**, and in complementary pie regions **b**, as described in the text. In the inner $2'$ the profile in b) is azimuthally averaged as in a).

r$> 2'$, although it is not a simple radial function. This is consistent with a closer inspection of the tail in the X-ray map that shows a highly irregular morphology (see Fig. 8). More detailed discussion of the properties of this galaxy will follow.

Although surface brightness profiles have traditionally been represented by a two parameter model (a core radius r_x and a radial dependence parameter β), the core radii in these galaxies are smaller than the PSF of the instrument, as suggested by the higher spatial resolution data of some of these (see for example Trinchieri et al 1986), so that determining r_x is not extremely meaningful. We have therefore fitted the radial dependence of

the profile at large radii with a simple power law fit (Table 2). Outside of a radius of $2'$ the influence of the PSF and of r_x are negligible. There is a large variety of radial dependencies of Σ_x, spanning from the flattest distribution of NGC2563 ($\Sigma_x \propto r^{-1.2}$) to the steepest NGC 4649 ($\Sigma_x \propto r^{-3.4}$).

2.2. Spectral data

As already shown by previous studies (Trinchieri et al 1994; Buote & Canizares 1994; Fabbiano et al 1994; Bauer & Bregman 1996) the spectral capabilities of ROSAT do not allow us
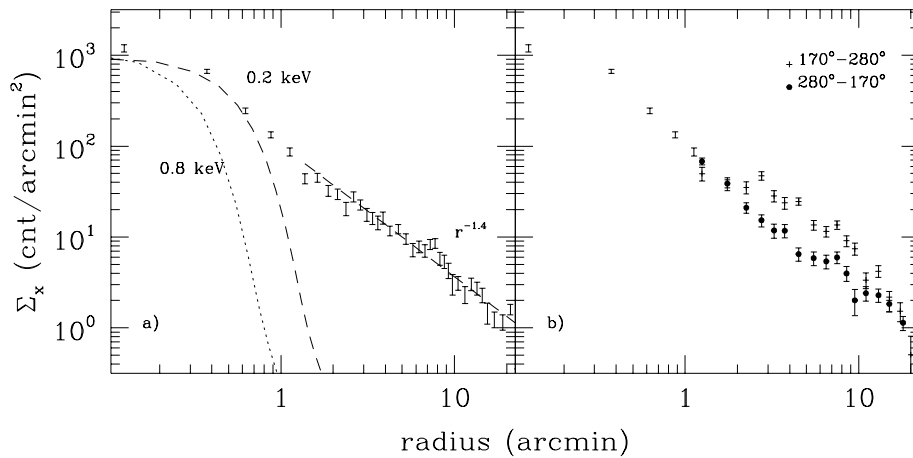
Fig. 5a and b. Radial surface brightness profile of the net X-ray emission of NGC7619, azimuthally averaged **a**, and in complementary pie regions **b**. In the inner $1'$ the profile in b) is azimuthally averaged as in a).

to measure the metallicity of the gas, since the results obtained from models of varying metallic contents are at best ambiguous. We have therefore assumed a thermal plasma model with low energy absorption and fixed the gas abundances at the cosmic value. We have however checked how much different abundances would affect the results obtained and discuss the results at the end of this section.

We have based the spectral analysis primarily on the IRAF/PROS software, which uses the same 34 channels of pulse height defined by the 'SASS' (see ROSAT Data Production Guide, by Downes, White and Reichert). To obtain the temperature in different regions, the data are extracted in concentric annuli of varying widths. The background is taken in a region considered free of emission, from the same field to ensure that its spectral distribution is the correct one for that particular observation, and is then corrected for differential vignetting before subtraction, as described in the PROS documentation. In general, the annulus at $25' - 27'$ from the field center has been used to estimate the background. Other choices made for NGC 4649 and the Pegasus field are discussed below. An average temperature, over the entire source, is also derived for completeness.

Tables 3a through 3e summarize the spectral results for each galaxy separately, graphically shown in Fig. 6. A cooler inner region, and a general tendency of increasing temperatures with galactocentric radii are seen, with the exception of NGC 2563, for which the temperature outside the inner $1'$ is isothermal at ~ 1.1 keV. For NGC 533 a drop in the temperature is also observed outside of a $6'$ radius, although with large errors.

There is no clear trend of varying low energy absorption with radius, with the exception of the central bin of NGC 4649, where the fitted values of N_H is higher than outside. Often however N_H is not very well constrained.

Briefly for each galaxy:

NGC 533 : The average gas temperature within $r \sim 6'$, *i.e.* before the radial profile becomes asymmetric, is ~ 1 keV, in the assumption of a 1-Temperature model. This however gives a relatively high χ^2_{min} value of 42.9 for 25 degrees of freedom (DOF), that is significantly lowered ($\chi^2_{min} \sim 19.6$) by adding a

second temperature in the model. The two best fit temperatures become kT_1=0.30-0.90 [at the 90% confidence limit] and $kT_2 >$ 1.2 keV. The suggestion that at least 2 temperatures are present in the data is well justified by the temperature profile obtained at different radii. In fact, when the emission is divided in 3 concentric annuli, the temperature increases from 0.9 [0.84-0.94] at the center to > 1.1 keV in the outermost bin.

If the whole $\sim 17'$ region is considered, the average temperature also is around 1 keV, however the errors become larger and the χ^2_{min} value does not require a two-temperature fit as in the case above.

NGC 2563 : The spectral distribution of the data obtained in the two observations have been compared to assure ourselves of their consistency, before merging the two data sets for the following analysis.

The average gas temperature within r=15' is kT~ 1.06 keV, with an acceptable $\chi^2_{min} = 24$ for 23 DOF. The temperature profile obtained in 7 concentric annuli indicates a cooler core in the inner $1'$ radius, and a constant ~ 1.1 keV value outside, although a possible indication of a temperature decrease with radius is visible in the data (see Fig. 6).

NGC 4649 : Given the uncertainty in the normalization of the background template, we have considered both the $25' - 27'$ annulus used for all other fields, and an annulus at $11' - 13'$ for background estimates. This latter choice has the advantage that the vignetting corrections are reduced. Moreover, if the Virgo cluster is responsible for the "extra" emission outside of $\sim 7'$, we would subtract it from the galaxy data. A comparison of the spectral distribution of the data in the two regions ($11' - 13'$ vs $25' - 27'$) however shows that they are consistent within the errors. In the present analysis we have chosen the $11' - 13'$ annulus as background.

The one temperature fit for the whole source within $r \sim 6'$ gives a best fit kT=0.85, with a χ^2_{min} of ~ 47.9 for 25 DOF. The introduction of a second model component lowers the χ^2_{min} to 30.5 for 23 DOF, and gives $kT_1 = 0.64$ - 0.84 keV, and $kT_2 > 1.2$

Table 3. Spectral Results for each Galaxy in different regions

Table 3a. NGC 533

Ann. (')	Net counts	Chan.	kT (keV)	90% confidence region	N_H (cm^{-2})	90% confidence region	χ^2_{min}	ν	Notes
0-1	1334.4±41.6	5-28	0.904	0.84-0.94	20.41	20.25-20.55	23.5	21	
1-3	812.7±36.9	5-30	1.074	0.99-1.22	20.23	20.05-20.40	16.2	23	
3-6	897.8±46.1	5-28	1.299	>1.07	20.22	<20.45	18.9	21	
6-10	985.8±63.9	5-28	0.941	0.83-1.08	19.74	<20.20	9.6	21	
10-17	353.6±41.3	5-8 10-25	1.024	>0.80	19.60	<20.20	12.2	17	
0-6	3093.0±70.7	5-32	1.028	0.98-1.07	20.26	20.20-20.35	42.9	25	
			0.552	0.30-0.90	20.33		19.6	23	1
			1.228	>1.2					

Table 3b. NGC 2563

Ann. (')	Net counts	Chan.	kT (keV)	90% confidence region	N_H (cm^{-2})	90% confidence region	χ^2_{min}	ν	Notes
0-1	1143.5±40.5	5-30	0.848	0.80-0.92	20.40	20.20-20.60	17.8	23	
1-3	1302.8±53.0	5-30	1.177	1.07-1.38	20.40	20.20-20.60	22.1	23	
3-5	1176.3±60.1	5-30	1.244	1.10-1.55	20.40	20.15-20.70	19.4	23	
5-7	1308.1±72.1	5-30	1.192	1.08-1.38	20.38	20.15-20.55	19.1	23	
7-9	1269.0±82.6	5-30	1.025	0.91-1.15	20.22	<20.70	20.7	23	
9-12	1867.4±116.6	5-10 13-30	1.075	0.97-1.27	20.00	<20.35	17.5	21	
12-15	1149.6±127.7	5-10 13-26	1.014	0.83-1.35	19.60	<20.60	15.3	17	
0-15	9050.1±312.0	5-30	1.058	1.01-1.14	20.20	20.00-20.40	23.9	23	

Table 3c. NGC 4649

Ann. (')	Net counts	Chan.	kT (keV)	90% confidence region	N_H (cm^{-2})	90% confidence region	χ^2_{min}	ν	Notes
0-1	3670.0±66.1	5-30	0.814	0.78-0.83	20.28	20.25-20.35	27.2	23	
			0.756	0.46-0.80	20.36	—	14.1	21	1
			2.91	>1					
1-2	1237.2±44.0	5-28	0.898	0.83-0.96	19.99	19.75-20.20	15.3	21	
2-3	463.8±34.8	5-7,9-29	0.923	0.78-1.08	19.74	<20.25	14.0	21	
3-6	388.7±61.7	6-9,11,12 14-26	1.315	>0.93	19.60	< 20.60	15.8	16	
0-6	5741.2±112.9	5-32	0.853	0.82-0.90	20.10	19.95-20.30	47.9	25	
			0.793	0.64-0.84	20.20	—	30.5	23	1
			3.000	> 1.2					

Table 3d. NGC 7619

Ann. (')	Net counts	Chan.	kT (keV)	90% confidence region	N_H (cm^{-2})	90% confidence region	χ^2_{min}	ν	Notes
0-1	972.4±36.8	5-30	0.775	0.70-0.82	20.59	20.40-20.85	12	23	
1-3	858.3±39.6	5-29	0.885	0.82-0.94	20.55	>20.25	17.6	22	
3-10	1073.6±49.1	6,7,9-30	0.948	0.88-1.02	20.41	20.10-21.10	19.2	21	2
0-10	2886.4±72.6	5-29	0.880	0.84-0.92	20.58	20.40-20.85	27.8	22	2
			0.812	0.60-0.88	20.67	—	19.5	20	1
			3.00	> 1.1					
"group"	2150.1±143.6	5-7,9 11-29	1.267	1.10-1.90	20.04	19.50-20.40	13.3	20	
									3

Table 3. (continued)

Table 3e. NGC 7626

Ann. (′)	Net counts	Chan.	kT (keV)	90% confidence region	N_H (cm^{-2})	90% confidence region	χ^2_{min}	ν	Notes
0-1	404.4±26.1	6-30	0.737	0.58-0.88	20.48	>20.20	18.9	22	
0-3	613.5±34.1	8-28	0.826	0.68-0.90	20.50		25.2	18	

Notes to the table. The line-of-sight N_H value is: ~ 20.5 for NGC 533; ~ 20.7 for NGC 2563, NGC 7619 and NGC 7626; ~ 20.4 for NGC 4649 (Stark et al 1992).

1 A two temperature fit is used. kT_1 and kT_2 are given on successive lines. The errors are derived for kT only

2 Limited to the $170°$-$280°$ sector in the $3' - 10'$ annulus.

3 "group" is the region from $2'$ to $16'$, centered on NGC 7619, and excluding the $170°$-$280°$ sector.
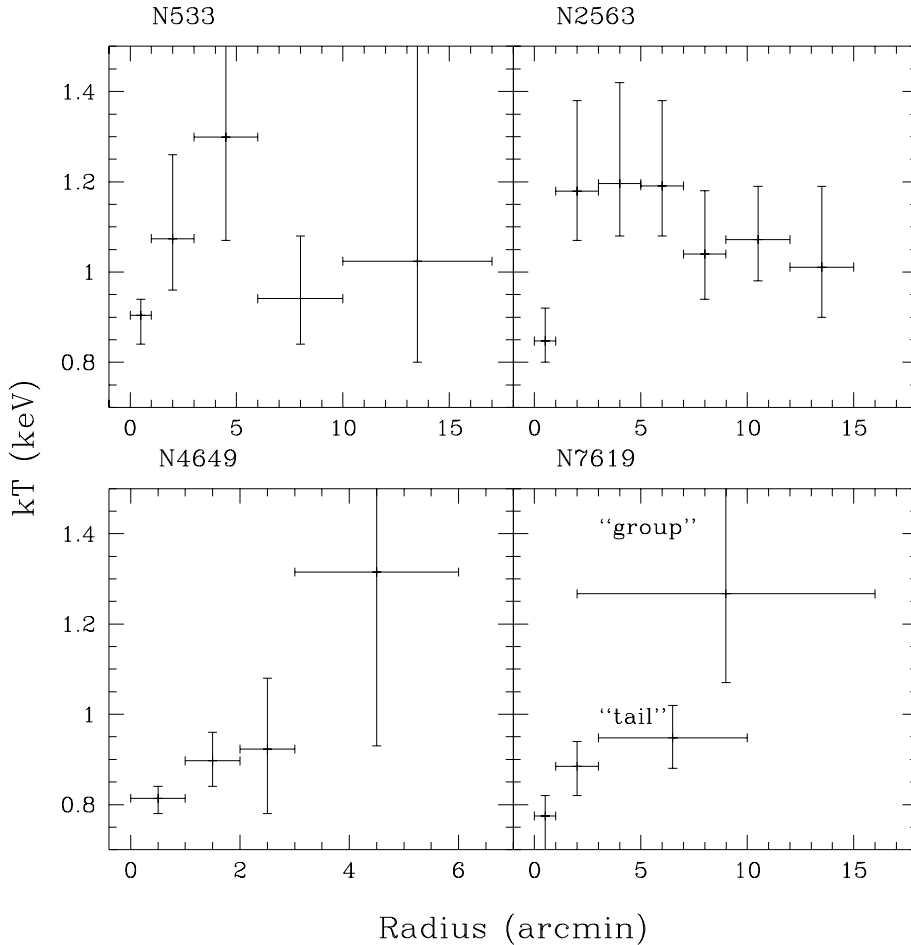
Fig. 6. Summary plot of the temperature parameters derived for different annular regions in the sample galaxies.

keV at the 90% confidence level. No further reduction of χ^2_{min} is achieved with the addition of a third component.

A slow increase of T towards large radii, and a higher value of the absorbing column in the innermost $1'$ circle are suggested by the data.

Pegasus I group : The contour map and the radial profile show that the emission from the Pegasus I group field covers the inner $20'$ circle, and it is likely to extend further out, with the possible exception of a region north of the NGC 7619 galaxy. We have

therefore tried both this region of low emission and the annulus at $25' - 27'$ for background estimates. The former choice would have the advantage of smaller corrections, but with a larger statistical uncertainty due to the smaller area covered. As for the case of NGC 4649 however, a comparison between the spectral distribution of the data in the two regions shows consistency within the statistical errors. We have therefore used the outer annulus as background in the following analysis.

The source associated with NGC 7619 has been divided into two annuli within r=$3'$, and the "tail", in the SW quadrant, from

$3' - 10'$. Table 3d indicates that there is a significantly cooler $1'$ core, and that the tail is harder than the galaxy. The group gas (in the $2' - 16'$ region, excluding the "tail") is also harder than the tail. The low energy absorption is not well constrained, and is in general consistent with the line of sight value.

NGC7626 extends only out to r$\sim3'$, and the total number of counts detected does not allow us to examine the spectral distribution of the data in different regions. The average temperature over the whole $3'$ circle is kT$\sim$0.83 keV with a χ^2_{min} of 25.2, which is entirely consistent with the temperature obtained from just the innermost $1'$ circle.

We have also examined the spectral distribution of the data of the galaxies above the possible cluster emission by assuming as background the annulus at $4' - 10'$ from the field center, with the exclusion of a $3'$ circle at the position of the two galaxies. The resulting best fit parameters are consistent with those reported in Table 3.

Metal Abundance In order to explore the effect of different abundance models on the temperatures derived, we have redone the spectral fits for a few of the cases presented in Table 3, where the statistics is higher, fixing the abundance parameter at 20% the cosmic value.

The absolute values of the temperatures are smaller (< 0.1 keV in all cases examined, and typically is $\sim 0.05 - 0.06$) and the low energy cutoff values are higher (typically, ~ 0.3 in log N$_H$) in the case of 20% abundances, but the trends and the uncertainties on T are preserved. The values of χ^2_{min} are also consistent with one notable exception, given by the global spectrum of NGC533 (in the $0' - 6'$ annulus). The 20% abundance model gives an acceptable χ^2_{min}=24 for kT=0.95 and N$_H$=20.6 (χ^2_{min}= 43 for the 1-temperature model at 100% cosmic abundance, Table 3). To obtain a similar χ^2_{min}, a 2 temperature model must be assumed for 100% cosmic abundances. This is however an indication of the ambiguity with which the spectral parameters can be derived from the limited spectral resolution of the ROSAT PSPC (cf. Fig. 7 in Trinchieri et al. 1994).

3. Derived quantities

3.1. Fluxes and luminosities

Table 4 summarizes the resulting fluxes and luminosities for the sample galaxies within the given radius R$_m$. The counts to flux conversion is derived from the parameters of the best fit spectral model of the source as a whole. However, the fluxes are entirely consistent with those obtained by summing the contribution of each annulus, accounting for the different spectral parameters obtained for each of them.

Luminosities are in the range L$_x \sim 2 - 60 \times 10^{41}$ erg s^{-1}, at the top of the distribution of X-ray luminosities of early type galaxies (see Fabbiano et al 1992).

3.2. Density profiles

The radial profiles, together with the spectral results, have been used to derive the radial dependence of intrinsic gas parameters: electron density, cooling time and total gas mass. Since the observed surface brightness profile is the integral along the line of sight, a deprojection of the observed quantity is needed to obtain the intrinsic distribution (Kriss et al 1993). However, the temperature of the gas must be known to derive its density, and the preceding analysis has only provided us with the projected values. A proper deconvolution of the spatial/spectral data is needed to derive this quantity. We have however approximated this procedure with the following assumptions: 1) the gas is assumed homogeneous, *i.e.* the gas has only one temperature at any given radius; 2) the temperature is constant in any given annulus; 3) the observed projected value of the temperature is not significantly different from the de-projected intrinsic value. This last assumption is supported by the results of the procedure used in the analysis of NGC4636 data. There Trinchieri et al (1994) had applied the same de-projection used to derive the intrinsic surface brightness distribution to the spectral data as well, and have derived the best fit parameters and errors based on the de-projected distribution. As can be seen from the comparison of their Tables 1, 2 and 5, the temperatures are consistent, within the errors. Moreover, it should be remembered that the density depends weakly on the temperature, therefore small changes in kT should not affect the results significantly. Finally, while assumption 1) is probably strictly incorrect, as the temperature is in most cases an increasing function of the radius, the increase is small and the data quality is such that this approximation should not be a serious source of error. Moreover, no correction for the effect of vignetting at large radii is applied (however the error introduced by this should be small).

The case of NGC4649: The density profile has been derived in the assumption that the emission outside of $7'$ should be considered background emission relative to the galaxy. This assumption is justified by its shape (see Sect. 2) and also by the fact that the galaxy is located in the Virgo cluster, relatively close to M87 (< 1 Mpc, for D=17 Mpc) where the cluster emission is still relatively strong (Boehringer et al 1994). The radial distribution of the net emission shown in Fig. 3 (panel b) also indicates that the profile flattens quite significantly outside of $7'$, when the background is taken far from the galaxy. This could be justified again by the presence of a low surface brightness emission such as that of a cluster gas.

The tail of NGC7619: An asymmetric feature is present to the SW of NGC7619. Even though the asymmetry is already present at a radius r$\sim 2'$, we have derived the density profile within a radius of $4'$ assuming azimuthal symmetry. This radius is estimated from the radial profile of the region complementary to the tail, and corresponds to a possible flattening of the profile.

The density profiles are shown in Fig. 7. Their parameterization is given in Table 5. Central densities span a relatively large range of value, 5-15 $\times10^{-3}$ cm $^{-3}$ [Note that these are probably underestimated due to the influence of the PSF which has not been removed]. This spread however could be due to

Table 4. Global Fluxes and Luminosities

| Galaxy	R_m^a ′ (kpc)	Counts[a]	Flux[b] erg cm^{-2} s^{-1}	L_x^b erg s^{-1}	D Mpc
NGC 533	18(565)	4321±115	4.19×10^{-12}	5.90×10^{42}	108
NGC 2563	20(560)	8612±220	2.28×10^{-12}	2.53×10^{42}	96
NGC 4649[c]	7(35)	5890±103	4.62×10^{-12}	1.61×10^{41}	17
NGC 4649[d]	17(84)	7418±197	5.82×10^{-12}	2.02×10^{41}	17
NGC 7619[e]	10(225)	2980±60	2.23×10^{-12}	1.51×10^{42}	75
NGC 7626	3.5(75)	623±34	4.21×10^{-13}	2.83×10^{41}	75

[a] The maximum radius R_m (in ′ and in kpc in parenthesis) and the counts given are consistent with the radial profiles of Fig. 3-5 in the energy range 0.14-2.00 keV.
[b] Single temperature fits have been used for all galaxies
[c] The background template is normalized to the data in the $11' - 13'$ annulus
[d] The background template is normalized to the data in the $25' - 27'$ annulus
[e] Azimuthally averaged for r≤ $3'$, and in the 170°-280° sector for $3'$< r ≤ $10'$
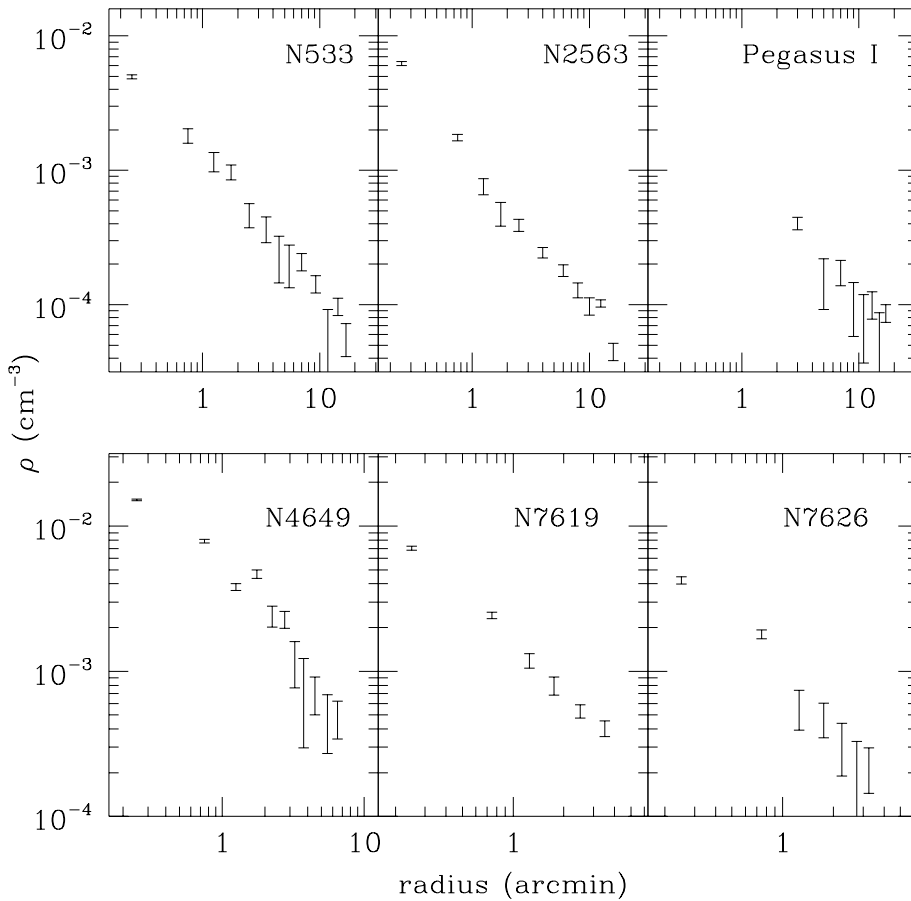
Fig. 7. Radial density distribution for the sample galaxies. The plot for Pegasus I refers to the intergalactic emission outside the "tail" feature of NGC7619 and outside the two bright galaxies NGC7619 and NGC7626.

the different distances of the objects, such that the inner 0.′5 circle in which the central densities are estimated refer to circles of radii 2.5 kpc, in NGC4649, and of 10 to 15 kpc for the others. Similarly, the outermost radii at which the densities are derived refer to significantly different physical sizes, from 35 kpc (NGC4649), to 90 kpc (NGC7619), to ≥ 500 kpc for the other galaxies.

Total gas masses and cooling times have also been derived, for a filling factor f = 1. Central cooling times range from ∼ 6 ×10^8 yr for NGC 7619 to ∼ 3 ×10^9 yr for NGC 533. At the outermost radius considered they are < 10^{11} yr for NGC 4649, NGC 7619 and NGC 7626, and ∼ 2-3 ×10^{11} yr for NGC 533 and NGC 2563. Total gas masses (listed in Table 5) again span a large range from M$_{gas}$ ∼ 4× 10^9 to ∼ 10^{12} M$_\odot$. At similar physical sizes (35 kpc), M$_{gas}$ are ≤ 10^{10} M$_\odot$ for all

Table 5. Total Mass, Gas Mass, Mass-to-Light ratio and "Visible"-to-total Mass fraction.

Name	R_m^a '(kpc)	$\Delta\rho^b$	ΔT^c	$T(R_m)^d$ keV	M_{gas} $M_\odot$	M_T^e $M_\odot$	M/L^f $M_\odot/L_\odot$	f^g %
NGC533	6(190)	-0.96±0.14	0.16±0.03	1.3	7.3×10^{10}	$7.3[\pm1.3]\times10^{12}$	50	20
NGC533	18(570)	-1.05±0.13	0	1.0	2.2×10^{12}	$2.2[\pm0.3]\times10^{13}$	70-160	20-15
NGC2563	15(420)	-0.81±0.06	0	1.1 ±0.15	1.3×10^{12}	$1.4[\pm0.2]\times10^{13}$	10-150	95-15
NGC4649	7(35)	-1.72±0.31	0.19±0.08	1.3	4.2×10^{9}	$2.6[\pm0.5]\times10^{12}$	50	16
NGC7619	4(90)	-0.96±0.20	0.10	0.89±0.05	4.7×10^{10}	$2.9[\pm0.6]\times10^{12}$	30	25
NGC7626	3.5(75)	-1.55±0.34	0	0.83±0.07	1.8×10^{10}	$3.6[\pm0.8]\times10^{12}$	40	20
Pegasus I	16(350)	-0.64±0.20	0	1.28±0.15	$\sim8\times10^{11}$	$1.1[\pm0.4]\times10^{13}$	60	20

Notes:

[a] Maximum radius (in ' and in kpc in parenthesis) at which the total mass M_T is calculated

[b] Density gradients. The slope of the density profile is calculated assumning a simple power law outside of r=2' to avoid the influence of the PSF except for NGC 7619 and NGC 7626, for which r_{in}=1'.5

[c] Temperature gradients, calculated assuming a simple power law fit. They are based on 3 points for NGC 533, on 4 points for NGC 4649 and on 2 points only for NGC 7626, for which no error on the fitted gradient is given.

[d] Temperatures at R_m. The errors are at the 68% confidence. For NGC2563, the value is an estimate of the average temperature from the results of Table 3. For NGC533 and NGC4649 no errors are given, since only a lower limit could be determined.

[e] Total mass within R_m. Proper error estimates could not be done and the errors quoted are probably underestimates (see text). They should be taken with caution.

[f] Mass to light ratios. For NGC 533 and NGC 2563 they have been estimated based on both the group (Bothun et al 1983, Geller and Huchra 1983) and on the galaxy only luminous mass, respectively.

[g] "Visible" to total mass fraction. For NGC 533 and NGC 2563 it is estimated based on both the group (Bothun et al 1983, Geller and Huchra 1983) and on the galaxy only optical luminosity, respectively.

except NGC4649, which appears to contain less gas than the other objects ($\sim$ 1/2).

3.3. Total mass determination

The temperature and density distributions can be used to estimate the total gravitational mass M_T, if the gas is assumed in hydrostatic equilibrium in the galaxy's spherically symmetric potential (Fabricant & Gorenstein 1983).

Table 5 summarizes the mass estimates for the galaxies in the present sample. These have been calculated within the maximum radii also listed in the table, using the results on temperatures and densities reported above and also listed in the table. However there are still several caveats associated with these estimates, which also prevent a reliable estimate of the errors on these quantities: a) the calculations are based on assumptions that are not exactly met (*e.g.* spherical symmetry); b) in most cases only a lower limit to the temperature could be derived at R_{max}; c) the uncertainty in the value of the temperature due to the assumption of cosmic abundances is not taken into account; d) the assumed R_{max} often does not reflect the maximum extent of the source, but it is for example the farthermost region at which the gas temperature could be determined; e) the linear fits to calculate temperature and density gradients are done using the actual values of the quantities, without taking into account their error; moreover, density gradients are derived assuming a power law fit to parametrize the data, which does not take into account possible effects of the PSF and r_x (although at large radii these should be negligeable) and does not take into

account the effect of the energy dependent vignetting at large off-axis angles. The formal errors on M_T listed in Table 5 are therefore an underestimate of the real errors associated with the data, since some of the uncertainties have not been taken into account. The uncertainty in determining M_T can therefore be estimated to be > 25%.

For NGC 533 we give two different estimates, within a radius of 6', within which we detect a temperature gradient, and within the maximum extent of this galaxy of 18'. This latter is calculated assuming isothermality. For the Pegasus I cluster we give two different estimates of M_T, one for the individual galaxies, within a radius of 4' for NGC 7619 and 3.'5 for NGC 7626, and one for the cluster, based on the density distribution derived in the 250° azimuthal region that avoids the X-ray tail (cf. Fig. 5).

Total masses span from $\sim 3 \times 10^{12}$ M$_\odot$ to $\sim 2 \times 10^{13}$ M$_\odot$. This large range of values once again reflects the much different scales of the X-ray emission, relative to the galaxy only (R$\sim$ 35 kpc, NGC4649) or to the group (R$\sim$ 400 kpc, NGC 2563).

Mass-to-light ratios (M/L) and the "visible" (*i.e.* stars, hot gas) to total mass fraction f have been calculated and are also given in Table 5. M/L values span from $\sim$ 20 for the NGC2563 group to 30-50 for individual galaxies to > 100 for NGC533. f is of the order of $\sim$ 20% for all systems, with the exception of Cancer, for which it could be as high as $\sim$ 100%.
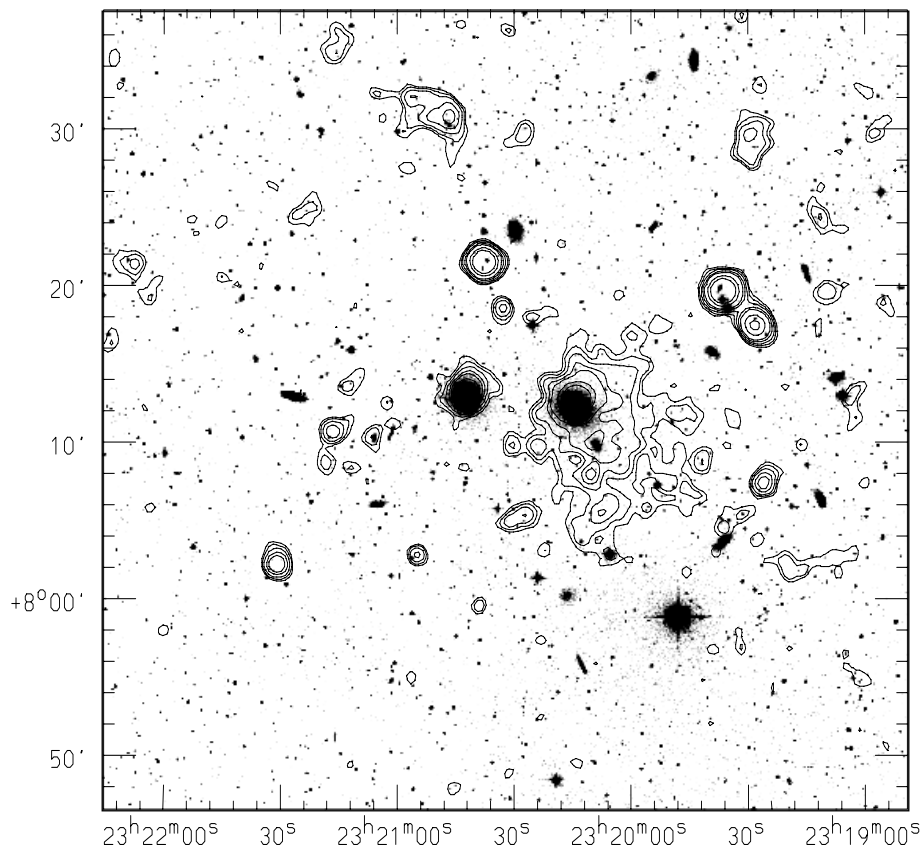
Fig. 8. Isointensity X-ray map of the Pegasus I group superposed onto the optical plate form the Digitized Sky Survey, smoothed with a gaussian function with $\sigma = 22''.5$.

4. The Pegasus I group

Fig. 8 shows the detailed X-ray emission from the Pegasus I group, superposed onto the optical plate of the area, from the "Digitized Sky Survey"[1]. The X-ray map shows that there is extended, low surface brightness emission in the area surrounding the two bright galaxies NGC 7619 and NGC 7626, that the emission is structured and that many clumps or other sources are present. Table 6 lists the counts rates for the clumps present. Counts are extracted in a circle of radius given in the table and the background is estimated locally from adjacent annuli. The positions are obtained from a combination of sources found by the detect algorithm and "eye-judgment" of the contour map. The luminosity of these "clumps" is in the range $1\text{-}10 \times 10^{40}$ erg s^{-1}, if they are at the Pegasus distance (75 Mpc).

Some of the X-ray structure is probably due to unrelated sources, most of which are coincident with optical candidates. It is clear from the map that most of the galaxies have no X-ray counterpart and vice versa, most of the X-ray sources or clumps of gas visible in the field are not associated with galaxies. The

Table 6. Sources in the Pegasus I field

Source	RA	δ	Radius	Counts	Err.	f_x
	J2000		$'$			erg cm^{-2} s^{-1}
1	23:19:26.2	8:07:25.2	0.83	76.34	11.6	3.9×10^{-14}
2	23:19:28.6	8:17:20.2	0.83	275.24	19.1	1.6×10^{-13}
3	23:19:37.0	8:19:31.1	1	724.14	29.9	3.2×10^{-13}
4	23:20:09.2	8:09:57.0	0.7	25.70	11.4	1.7×10^{-14}
5	23:20:11.0	8:07:54.1	0.67	42.96	11.0	1.8×10^{-14}
6	23:20:32.9	8:18:30.5	0.83	37.66	10.2	1.6×10^{-14}
7	23:20:38.0	8:21:25.5	1	693.25	28.6	2.4×10^{-13}
8	23:20:46.5	8:30:54.2	1	78.17	13.4	4.7×10^{-14}
9	23:20:55.1	8:02:45.5	0.67	43.16	9.0	2.7×10^{-14}
10	23:21:16.7	8:10:30.3	0.83	51.30	10.7	2.4×10^{-14}
11	23:21:31.5	8:02:05.2	0.83	76.49	11.1	4.2×10^{-14}

only notable exception, besides the two galaxies NGC7619 and NGC7626 already discussed, is NGC 7617, an S0 galaxy of $m_B = 14.8$, clearly coincident with a peak of emission in the tail of NGC 7619. The excess counts for this source (# 4 in Table 6) are estimated on a $0.7'$ circle at the position of the galaxy, above the local background, estimated in an annulus of $0.7' - 2'$ inner and outer radii respectively concentric to the source region. If the excess is attributed to the galaxy, NGC7617 would have an X-ray luminosity of 1.3×10^{40} for a 1 keV thermal

spectrum (appropriate for an early type galaxy) and line-of-sight column density. The X-ray-to-optical flux ratio of 30.1 would put this galaxy among the low X-ray luminosity galaxies, *i.e.* those galaxies in which the gaseous component does not dominate the emission (if it is present at all, see Fabbiano et al 1992).

The correspondence with NGC 7617 could alternatively be interpreted as chance coincidence, and this X-ray enhancement, together with the irregular appearance of the tail morphology, as inhomogeneities in the tail of NGC 7619. Similar inhomogeneities have already been reported in the emission of NGC507 (Kim & Fabbiano 1995), A85 and A496 (Prestwich et al 1995) and NGC1399 (Kim et al 1995) among others. A spectral analysis of such features in other groups indicates that they might be cooler denser condensations in the hot gas. Unfortunately, given the limited statistics of this observation, we can only measure the global spectral characteristics of the tail in the Pegasus I group. Cooler condensations could be the signature of density inhomogeneities induced by thermal instabilities, possibly triggered by dynamical effects. The evidence of a tail-type emission in NGC7619 would also point to dynamical effects, like stripping of gas as the galaxy moves into the denser cluster medium (the first example of a similar feature observed in NGC4406 was in fact interpreted as the result of the dynamical interaction with cluster gas, Forman et al 1979).

An intergalactic medium is known to be present from *Einstein* observations of this region (Canizares et al 1986), and it is also visible in the contour map of Fig. 8 and in the radial profile of Fig. 5 out to a radius of $\sim 16' - 20'$ from the galaxy's center (the background template has been normalized outside of this region, therefore no excess can be measured at larger radii, see Sect. 2.1). To avoid the obscuration due to the PSPC support structure, we have however restricted our estimate of the diffuse group emission to r $\sim 16'$. In the region comprised between $2'$ and $16'$ centered on NGC 7619 and excluding the sector containing the tail ($170°$-$280°$), a $2'$ circle around NGC 7626, and the other possible interlopers, we find about 2000 excess counts. If we correct for the area excluded, we estimate a total of ~ 3200 counts in the full $16'$ circle. The spectrum of this emission is consistent with a thermal model with kT=1.1-1.9 kT (90% confidence). The flux, $f_x \sim 2.5 \times 10^{-12}$ erg cm^{-2} s^{-1}, corresponds to $L_x = 1.7 \times 10^{42}$ erg s^{-1} (D = 75 Mpc), comparable to the luminosity of the NGC7619 complex emission.

To estimate the density of the intergalactic gas, the tridimensional spatial distribution must be known. Assuming spherical symmetry, and filling factor of unity, we have derived an average density of $\sim 1.9 \times 10^{-4}$ cm^{-3}. This is probably an underestimate of the real gas density in the group since the emission does not seem to fill uniformly the observed surface (a circle of r=16$'$). The corresponding total mass of gas in the same volume is $M_{gas} \sim 8 \times 10^{11}$ M$_\odot$.

These results are entirely consistent with the estimates based on the *Einstein* data (Canizares et al 1986), and with those summarized for a sample of poor clusters of galaxies by Price et al (1991), also based on *Einstein* data.

**Table 7.** Sources in the NGC 2563 field

Source	RA	δ	Radius	Counts	Err.	f_x
	J2000		$'$			erg cm^{-2} s^{-1}
1	8:18:38.5	20:46:43.7	1.5	92.34	28.79	3.80×10^{-14}
2	8:18:40.3	21:02:16.6	1.5	325.00	34.78	1.22×10^{-13}
3	8:18:52.6	21:23:25.3	1.5	155.03	29.54	6.15×10^{-14}
4	8:18:58.7	21:26:03.8	0.7	79.68	30.35	3.20×10^{-14}
5	8:19:13.2	21:10:50.7	0.7	52.29	11.22	1.78×10^{-14}
6	8:19:17.9	21:02:32.1	1.5	92.52	14.44	3.09×10^{-14}
7	8:19:28.9	21:10:49.5	1.5	129.16	28.40	4.22×10^{-14}
8	8:19:34.6	20:57:09.8	0.7	77.80	14.37	2.53×10^{-14}
9	8:19:37.1	20:42:58.9	1.5	296.93	31.58	1.09×10^{-13}
10	8:19:40.2	21:06:26.3	0.7	71.11	14.06	2.23×10^{-14}
11	8:19:47.1	21:18:13.5	0.7	61.85	12.42	2.05×10^{-14}
12	8:19:52.0	20:59:11.1	0.7	54.04	12.94	1.75×10^{-14}
13	8:19:52.9	21:01:32.3	0.7	54.04	13.17	1.64×10^{-14}
14	8:19:58.6	21:07:02.2	0.7	176.47	18.09	5.29×10^{-14}
15	8:20:02.5	20:55:28.4	0.7	71.18	13.82	2.17×10^{-14}
16	8:20:18.0	21:13:35.4	0.7	68.85	13.84	2.09×10^{-14}
17	8:20:20.0	21:05:07.6	0.7	42.87	13.91	1.26×10^{-14}
18	8:20:21.9	21:08:04.3	0.7	42.78	14.07	1.25×10^{-14}
19	8:20:30.6	20:56:15.7	0.7	58.06	12.91	1.74×10^{-14}
20	8:20:33.2	21:24:47.2	1.5	113.00	25.37	3.86×10^{-14}
21	8:20:42.1	20:57:19.3	0.7	265.74	20.28	7.88×10^{-14}
22	8:20:43.4	21:08:30.8	0.7	36.06	13.38	1.06×10^{-14}
23	8:21:01.5	21:28:48.5	1.5	139.56	25.57	5.10×10^{-14}
24	8:21:02.6	20:47:31.8	1.5	451.97	32.69	1.50×10^{-13}
25	8:21:07.1	21:17:27.0	0.7	41.93	12.33	1.36×10^{-14}
26	8:21:24.7	21:27:26.0	0.7	117.98	28.14	4.36×10^{-14}
27	8:22:14.9	21:05:41.2	1.5	215.81	28.10	7.73×10^{-14}

Table 6 reports the presence of 10 'other' sources in the field. As already mentioned, there are no associations between these X-ray clumps and galaxies. However, most of them are coincident with an optical counterpart on the "Digitizes Sky Survey". The total number of sources detected moreover is entirely consistent with the expected number from the LogN-LogS function of Hasinger et al (1993).

5. NGC 2563 – The Cancer subgroup A

The X-ray emission shown in Fig. 9 is centered on NGC2563, the brightest galaxy in the largest of the subgroups (Group A) that constitute the Cancer cluster (Bothun et al 1983). As shown by the figure (a superposition of the X-ray contours over the "Digitized Sky Survey" plate of the area), there are secondary peaks of emission, several of which, unlike in the case of the Pegasus I group, coincide with galaxies. The net counts associated to these peaks are listed in Table 7.

Counts are extracted in circles of 0.$'$7 or 1.$'$5 radii (smaller for sources in denser/more confused area), and the background is estimated from an adjacent annulus. The positions are obtained from a combination of the peaks found by the detect program and "eye-judgment" of the contour map. If these sources
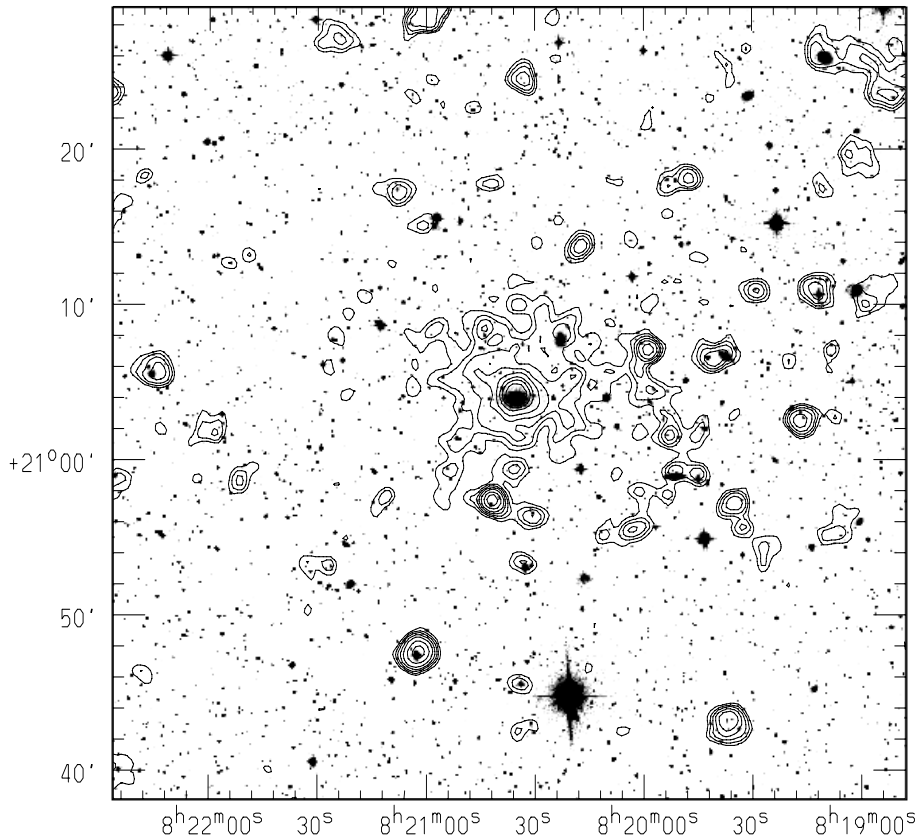
Fig. 9. Isointensity X-ray map of the Cancer subgroup A (NGC2563) superposed onto the optical plate form the Digitized Sky Survey. A smoothing function with $\sigma = 22.''5$ is applied to the data.

are at the distance of NGC2563, their luminosities (1 keV spectrum with line-of-sight column densities) are in the range $\sim 10^{40} - 10^{41}$ erg s^{-1} consistent with the luminosities of normal galaxies. However, not all of the clumps are associated with galaxies, and vice versa, not all galaxies are associated with clumps in the X-ray emission. Therefore a direct association clumps-galaxies must be made with some caution. In particular, as already mentioned for the case of the Pegasus I group, inhomogeneities have been observed in other groups and clusters, apparently not associated with optical objects. The 'sources' N. 4, 6, 12 and 18 appear to coincide with early type galaxies of the Cancer subgroup A (Zw 119048, 119053, 119058, 119063 respectively), and source 27 coincides with an early type galaxy of subgroup B (Zw 119072). Source 10 is associated to a late type galaxy (Zw 119055), also from subgroup A. Most of the other clumps appear to coincide with one or more object in the "Digitized Sky Survey" plate. A detailed analysis of the spectral properties of these sources cannot be done at this stage, due to the limited statistics available.

The contour map of Fig. 9 indicates that the extended emission is probably associated only to Group A, and should be assigned a distance based on the 4705 km s^{-1} velocity that Bothun et al (1983) have estimated for that group. The presence of a clump of emission around source 27, associated with a galaxy in Group B, might indicate that this subgroup also has X-ray emission. Unfortunately, the present observation is not deep enough to study it in details (Group B is also at a much

higher average velocity, v=6326 km s^{-1}). At the distance of 126.5 Mpc, $L_x \sim 1.5 \times 10^{41}$ erg s^{-1}.

The radial distribution of the emission (Fig. 3) is one of the flattest of the present sample of galaxies and is very similar to other radial distributions reported for galaxy groups (NGC 507, Kim & Fabbiano 1995; NGC 1399, Kim et al 1995). It is therefore likely that the group emission dominates also in this case outside of the inner 1' (30 kpc) $i.e.$ outside of the optical size of the galaxy, as measured by the UGC (Nilson 1973). The temperature profiles also indicates that the gas is isothermal outside of the inner 1′ region, where a cooler galaxy gas is found.

As shown by Table 5, to NGC2563 is associated the largest gravitational mass we have calculated. The total mass, $M_T \sim 10^{13}$ M$_\odot$, is comparable with the total masses estimated for other groups of galaxies (NGC5044, David et al 1994; NGC507, Kim & Fabbiano 1995; NGC4261, Davis et al 1995). However, our estimate is about a factor of 10 less than that derived from the dynamical properties of the group, as estimated by Bothun et al (1983). If we use our mass estimate, we can calculate the mass-to-light ratio both for the group as a whole ($i.e.$ taking into account all of the optical light as given by Bothun et al.) and for the single galaxy ($i.e.$ assuming that the whole X-ray emission should be attributed to NGC2563). This results in M/L in the range 10-150 respectively.

6. Other galaxies in the observed groups

The present observations of the two groups (Pegasus and Cancer) are much more sensitive than those obtained with the *Einstein* instruments. The Cancer field in particular has been observed for 50000 sec., which allows us to detect sources as faint as $\geq 2 \times 10^{-14}$ erg cm^{-2} s^{-1}. This corresponds to a luminosity $L_x \sim 10^{40}$ erg s^{-1}, for the spectral parameters of Table 6 at the assumed Cancer distance. In the NGC533 field, NGC521, a bright late type galaxy in the same group (GH14, Geller & Huchra 1983) is also detected with $f_x \sim 1.4 \times 10^{-13}$ erg cm^{-2} s^{-1}, corresponding to $L_x \sim 2 \times 10^{41}$ erg s^{-1} (for a 5 keV thermal bremsstrahlung spectrum, with line-of-sight absorption). As already noticed, besides the targets, 6 of the galaxies in Cancer (5 early and one late types) and one (early type) in Pegasus have been individually detected, at fluxes $f_x \geq 2 \times 10^{-14}$ erg cm^{-2} s^{-1}. This corresponds to X-ray luminosities in the range $1\text{-}10 \times 10^{40}$ erg s^{-1}, entirely consistent with the X-ray luminosities of normal galaxies (Fabbiano et al 1992). Moreover, these are among the optically brighter objects. Therefore, given the observed trend that brighter galaxies are also on average more X-ray luminous, the lack of detection of all galaxies is entirely consistent with this trend and with the related scatter.

If the association of the excess counts with the corresponding optical galaxy is real, the X-ray to optical ratio for these objects spans from a value of ~ 29.6 for NGC2562 (source 18 in Cancer) to ~ 31 for source 27 in Cancer, associated with a Group B galaxy (ZW119072), *e.g.*, they cover the entire range observed for early type galaxies (Kim et al. 1992).

7. Conclusions

ROSAT PSPC observations of 5 X-ray bright early-type galaxies are analyzed and the spectral characteristics of the X-ray emitting hot gas that dominates the emission are derived.

The morphology of the gas appears in most cases to deviate from azimuthal symmetry, indicating that the assumption of spherical symmetry is often an oversimplification of the real distribution of the gas. Several clumps or additional sources are also observed, some of which could be related to the presence of a group emission. In the NGC2563 field several of this seemingly unrelated sources appear to coincide with galaxies in the group. Whether these are detections of individual galaxies or whether they are substructures of the group gas that coincide with the presence of a galaxy is not known. However, if these are individual galaxies, their X-ray luminosity is consistent with those of normal galaxies of the same optical luminosity (cf. Fabbiano et al 1992).

We find that the gas has an average temperature of 0.8-1 keV, and that a positive temperature gradient is suggested in a few cases. However care must be taken when comparing temperatures for different systems, since they have been sampled over very different physical regions. In NGC4649, a bright galaxy in the Virgo cluster, the gas temperatures are estimated within a 35 kpc radius, and therefore we are most certainly in the galaxy itself. In NGC2563, at the center of group A in the Cancer cluster, the observed X-ray emission extends out to ~ 400 kpc and is probably due to the whole group, while the galaxy gas only contributes (and possibly dominates) in the inner $1'$ region (corresponding to a linear size of 35 Kpc), where a cooler temperature is also measured. Likewise, it is difficult to assess the presence of temperature gradients in galaxies, until the ambiguity between galaxy and group emission can be resolved. If positive gradients are present only in the gas of the galaxy proper (as is the case for example of NGC 4636; Trinchieri et al 1994), then a fair comparison between objects calls for spatially resolved spectra over the same linear size, which is only achievable at the present time for a handful of the most nearby, brightest objects. Until instruments with the appropriate spatial resolution coupled with high sensitivity and spectral capability become available (such as AXAF) we are not likely to resolve the issue of what are the properties of the emission from gas dominated early type galaxies compared to those of more complex systems (groups and clusters).

The determination of temperatures and densities at different radii could in principle be used to estimate the total mass of the system. However, at large radii, where a mass measure would be most interesting, temperatures are not well determined, and often only lower limits could be derived. Estimates of the total mass therefore remain highly uncertain. Formal values are in the range of a few $\times 10^{12}$ M$_\odot$ for individual galaxies to a few $\times 10^{13}$ M$_\odot$ for groups. This leads to M/L values of $\sim 30\text{-}100$ and to a "visible" to total mass fraction of the order of $\sim 20\%$ for all systems. The Cancer group seems to be an exception, with a "visible" mass that could be as high as $\sim 100\%$ of the total. However, as already discussed, the X-ray derived M_T is significantly smaller than that derived from dynamical considerations (Bothun et al 1983). The X-ray derived mass is in good agreement with similar results for other poor groups of similar dynamical properties (*i.e.* similar velocity dispersion). Since we are not aware of a systematic comparison between total mass derived from X-ray or dynamical methods for poor groups, this discrepancy could be also found in other systems.

References

Bauer, F. & Bregman, J.N. 1996, ApJ, in press
Boehringer, H, Briel, U.G., Schwarz, A., Voges, W., Hartner, G. & Truemper, J 1994, Nature, 368, 828
Bothun, G., Geller, M., Beers, T., Huchra, J., 1983 ApJ, 268, 47
Buote, D.A. & Canizares, C.R.C. 1994 ApJ 472, 86
Canizares, C.R.C., Donahue, M., Trinchieri, G., Stewart, G., and McGlynn, T. 1986 ApJ 304, 312
Chapman, G.N., Geller, M.J. and Huchra, J.P. 1988 AJ 95, 999.
David, L.P., Jones, C., Forman, W., and Daines, S. 1994 ApJ 428, 544
Davis, D., Mushotzky, R.F., Mulchaey, J.S., Worral, D.M., Birkinshaw, M., Burstein, D. 1995, ApJ 444, 528
Fabbiano, G. Kim, D-W. and Trinchieri, G. 1994 ApJ 429, 94
Fabbiano, G., Kim, D-W., and Trinchieri, G. 1992, ApJS 80, 645

Fabricant, D., Gorenstein, P 1983, ApJ 267, 535.

Forman, W., Schwarz, J. Jones, C., Liller, W., & Fabian, A.C. 1979, ApJL 234, L27.

Geller, M, Huchra, J, 1983, ApJS 52, 61

Hasinger, G. Burg, R., Giacconi, R., et al 1993, AA 275, 1

Kim D-W., Fabbiano G., & Trinchieri G. 1992 ApJ 393, 134.

Kim D.-W. & Fabbiano, G. 1995 ApJ 441, 182.

Kim D-W., et al, 1995, preprint

Kriss, G.A., Cioffi, D.F. & Canizares, C.R. 1983, ApJ 272, 439.

Nilson, P., 1973, "Uppsala General Catalogue of Galaxies", Uppsala Obs.Ann., Vol 6

Pfeffermann, E. at al 1987, Proc. SPIE 733, 519.

Prestwich, A.H., Guimond, S.J., Luginbuhl, C.B., and Joy, M. 1995, ApJ 438, L71

Price, R. Burns, J.O., Duric, N., Newberry, M.V. 1991 AJ 102, 14

Stark, A.A, Gammie, C.F., Wilson, R.W., Bally, J., Linke, R.A., Heiles, C., Hurwitz, M. 1992, ApJS 79, 77

Trinchieri, G., Fabbiano, G., & Canizares, C.R.C. 1986, ApJ, 310, 637

Trinchieri, G., Kim, D-W., Fabbiano, G., & Canizares, C.R.C. 1994, ApJ 428, 555

Truemper, J. 1983. Adv. Space Res. 2, No. 4, 241.